



# Plasma Induced Addition of Active Functional Groups to Biochar for Elemental Mercury Removal

Huicong Zhang<sup>1</sup> · Tao Wang<sup>1</sup> · Zifeng Sui<sup>1</sup> · Yongsheng Zhang<sup>1</sup> · Pauline Norris<sup>2</sup> · Baomin Sun<sup>1</sup> · Wei-Ping Pan<sup>1,3</sup>

Received: 4 April 2019 / Accepted: 19 July 2019 / Published online: 7 August 2019  
© Springer Science+Business Media, LLC, part of Springer Nature 2019

## Abstract

The mercury removal capacity of biochar can be improved by plasma modification and the functional group is an important factor affecting the mercury removal. This paper examines factors such as discharge voltages, gas flow rates, chlorine concentrations and discharge times that may affect functional groups on the surface of biochar. The mercury removal performance of the tobacco stem biochar prepared under different Cl<sub>2</sub> plasma modification conditions was investigated using a fixed bed reactor. The number of C–Cl bonds and carboxyl increased after modification and decreased in mercury removal. Longer discharge times can destroy the biochar surface and possibly cause a decrease in the number of active sites. Increasing the discharge voltage promotes the formation of C–Cl bonds and carboxyl groups. Excessive gas flow rates cause active chlorine to be carried out of the reactor quickly which reduces the formation of C–Cl. The amount of C–Cl bonds increases with increased chlorine concentration. In the modified biochar, C–Cl and carboxyl take part in the adsorption of mercury to form HgCl<sub>2</sub> and HgO, while the unmodified biochar is mainly physically adsorbed Hg<sup>0</sup>. C–Cl is the main functional group participated in mercury removal and the carboxyl is a secondary functional group. The proportion of HgCl<sub>2</sub> is at least 68.2% in the used modified biochar. Under optimum conditions, the initial mercury removal efficiency of modified tobacco biochar was 99.1%, and the efficiency was still 79.1% after 100 min.

**Keywords** Mercury removal · Biochar · Plasma · Chlorine · Carboxyl

---

✉ Tao Wang  
wangtao0420@163.com

✉ Yongsheng Zhang  
yszhang@ncepu.edu.cn

<sup>1</sup> Key Laboratory of Condition Monitoring and Control for Power Plant Equipment, Ministry of Education, North China Electric Power University, Beijing 102206, People's Republic of China

<sup>2</sup> Advanced Materials Research Institute, Western Kentucky University, Bowling Green, KY 42101, USA

<sup>3</sup> ICSET Solutions, Bowling Green, KY 42104, USA

## Introduction

Although activated carbon has good mercury adsorption capabilities, it is expensive [1]. The materials used to produce biochar in China are very abundant and inexpensive. Thus, biochar is an attractive alternative to activated carbon. Plasma modification is a simple, inexpensive method that produces a material with good adsorption properties [2–9]. Gas molecules are very active in a plasma environment [10, 11]. It is easier to break the gas molecular bond and form new bonds with biochar [12].

Halogen elements (I, Cl, Br) are often considered as methods for improving the mercury removal performance [13, 14]. Li [15] and Shen [16] used  $\text{NH}_4\text{Cl}$  to modify biochar to obtain C–Cl. They found that C–Cl is the main functional group consumed during the mercury removal process and to form  $\text{HgCl}_2$ . According to our previous and other scholars' research [17, 18], plasma techniques can be used to increase the number of chlorine active sites on biochar. The C–Cl bond is also considered to be the main functional group supporting the mercury removal process. However, Chen [19] and Tsai et al. [20] found that the oxygen functional groups on the materials also increased in a non-oxygen plasma environment. Our previous research [17] also found that the number of oxygen-containing functional groups on the surface of biomass carbon increased in the chlorine plasma environment. Oxygen functional groups (ester, carboxyl, hydroxyl, etc.) have been shown to promote mercury removal in many literatures [21, 22]. It is unclear whether the oxygen functional groups generated in the plasma environment participate in mercury removal. Thus, the synergistic effect of C–Cl bond and oxygen functional group on mercury removal by chlorine plasma modified biochar need to be clarified.

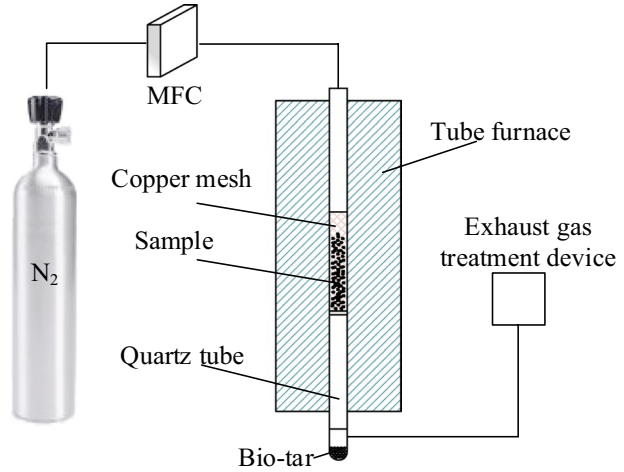
This study will investigate the changes in C–Cl and oxygen-containing functional groups in the case of different discharge voltages, gas flow rates, chlorine concentrations and discharge times. The effects of these changes on mercury removal performance will be explored.

## Materials and Methods

### Biochar Preparation

The schematic of biochar preparation device is shown in Fig. 1. Tobacco stems (TS) were collected from Henan, China. The TS material was washed three times with deionized water and dried in an oven set at 80 °C for 24 h. Then, the TS material was pulverized in the coal mill and sieved into 100–200 mesh. About 10 g of the TS sample (100–200 mesh) was wrapped in a copper mesh and the copper mesh was rolled to form a cylinder shape. Next, the cylinder was placed into a quartz tube in a muffle furnace. The sample was heated from room temperature to 600 °C in 1 h, then held for 1 h at this temperature and finally cooled to room temperature. The entire heating and cooling process were carried out in a nitrogen atmosphere flowing at 300 mL/min. The prepared TS biochar (TS-BC) was sieved to 200–350 mesh.

**Fig. 1** Schematic of biochar preparation device



**Modification of Biochar**

The biochar modification device consists of a mass flow controller (MFC), dielectric barrier discharge (DBD) plasma reactor, voltage regulator and exhaust gas treatment device. The schematic of plasma modification device is shown in Fig. 2. The plasma reactor was a hollow quartz disc with a diameter of 70 mm and a thickness of 10 mm. The upper and lower sides of reactor were sealed by a quartz disc having a thickness of 1.5 mm. Adjacent to the upper and lower quartz disc are two electrodes with a diameter of 50 mm. When the two electrodes are loaded with a sufficient voltage, a breakdown discharge occurs between the two electrodes, thereby generating a plasma. The left and right ends of the plasma reactor are the inlet and outlet of the modified gas respectively. The DBD output voltage range is 0–30 kV. The discharge frequency is 10 kHz. The biochar is placed in a plasma reactor and a modified gas is introduced. DBD is then performed to modify the biochar. TS biochar (0.3 g) was added to the DBD plasma reactor which was sealed with high-vacuum silicon grease. Before modification, nitrogen was

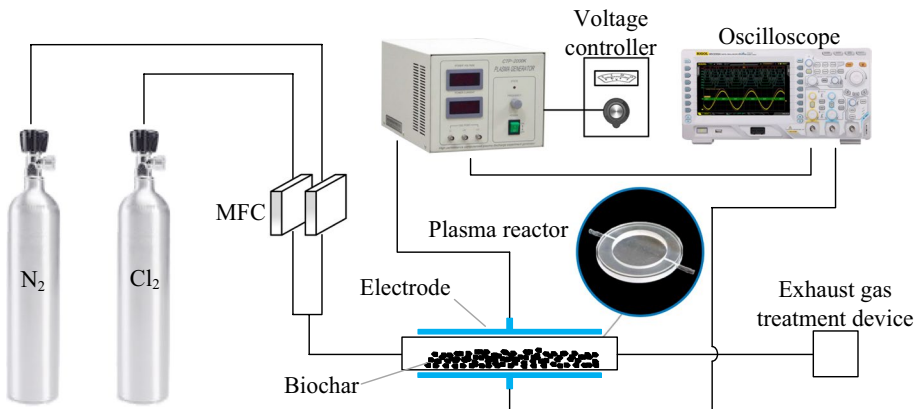


**Fig. 2** Schematic of plasma modification device

introduced into the system at 300 mL/min for 3 min to ensure an inert atmosphere. By adjusting the volume flow meter, different concentrations of chlorine gas flowed into the plasma reactor. Then, the voltage was varied so that the plasma reactor produced different breakdown effects. Experiments to change the discharge voltage, gas flow rate, chlorine concentration, and discharge time were named TS-V, TS-R, TS-C, and TS-T, respectively. The TS biochar modification parameters are provided in Table 1.

## Char Characterization

The sample surface area was measured by Quantachrome Autosorb-iq-MP using a nitrogen adsorption/desorption method at  $-196\text{ }^{\circ}\text{C}$ . The functional groups on the sample surface were characterized by Fourier transform infrared (FTIR) spectroscopy (PerkinElmer). The surface morphology was observed using a Hitachi S4800 Scanning electron microscope (SEM). X-ray photoelectron spectroscopy (XPS) was used to analyze the elemental states change of Cl and O on the surface of the biochar samples. The form of mercury after adsorption in biochar was tested by temperature programmed desorption (TPD). A Minitab 17 was used to analyze the degree of influence of the four parameters on mercury removal performance.

## Mercury Adsorption Experiment

The mercury adsorption experiment was performed using a laboratory-scale fixed bed, as shown in Fig. 3. Elemental mercury was generated using a PSA CAVKIT system. Air carried the elemental mercury out of the PSA CAVKIT system where it was mixed with

**Table 1** Tobacco stem biochar modification conditions

Name	Discharge voltage (kV)	Discharge time (min)	Gas flow rate (mL/min)	Chlorine conc. (%)
TS-V0	0	5	300	1
TS-V2	2	5	300	1
TS-V4	4	5	300	1
TS-V6	6	5	300	1
TS-V8	8	5	300	1
TS-R100	8	5	100	1
TS-R300	8	5	300	1
TS-R500	8	5	500	1
TS-R700	8	5	700	1
TS-C0	8	5	500	0
TS-C0.3	8	5	500	0.3
TS-C0.6	8	5	500	0.6
TS-C1	8	5	500	1
TS-T1	8	1	500	1
TS-T5	8	5	500	1
TS-T10	8	10	500	1
TS-T20	8	20	500	1
TS-T30	8	30	500	1

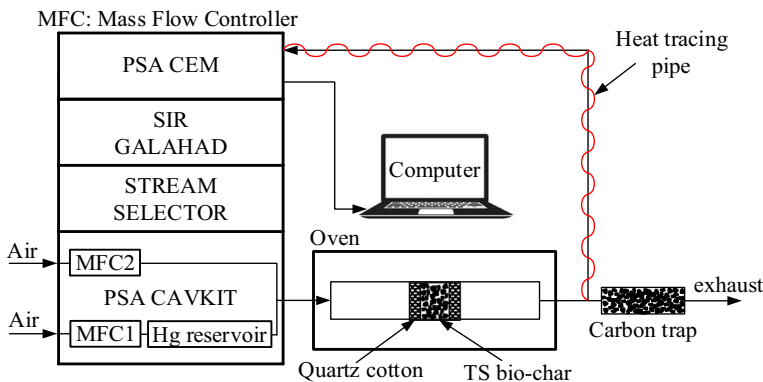


**Fig. 3** Schematic of mercury adsorption experimental device

compressed air. The released mercury concentration was controlled via computer at  $20 \mu\text{g}/\text{m}^3$  and the total gas flow was kept at 1 L/min. A 50 mg biochar sample was placed in a glass tube with an internal diameter of 4 mm and fixed with quartz wool. The bench temperature was kept at  $30 \text{ }^\circ\text{C}$ . The PSA CEM draws exhaust gas every 5 min to measure the mercury content. The results are displayed on the computer. The tubes leading to the CEM were heated to  $140 \text{ }^\circ\text{C}$  with heating trace pipe to prevent mercury condensation. The exhaust gas was filtered through a carbon trap and then discharged into the atmosphere. Each experiment was repeated three times and the result was the average of three results.

The  $\text{Hg}^0$  removal efficiency can be calculated by Eq. (1) [23–25].

$$\eta = \frac{C_{in} - C_{out}}{C_{in}} \times 100\% \tag{1}$$

where  $\eta$  is the efficiency of  $\text{Hg}^0$  removal (%),  $C_{in}$  is inlet concentration of mercury ( $\mu\text{g}/\text{m}^3$ ),  $C_{out}$  is outlet concentration of mercury ( $\mu\text{g}/\text{m}^3$ ).

The mercury accumulative adsorption amount per gram of samples can be calculated by Eq. (2) [26–28].

$$q_t = \frac{Q \int_0^t (C_{in} - C_{out}) dt}{M} \tag{2}$$

where  $q_t$  represents the adsorption mass of  $\text{Hg}^0$  ( $\mu\text{g}/\text{g}$ ) at reaction time  $t$  (min),  $Q$  is the total gas flow rate ( $\text{m}^3/\text{min}$ ),  $M$  is the biochar sample weight (g),  $t$  represents the adsorption time (min).

### Mercury Desorption Experiment

The sample is placed in a furnace to liberate various forms of adsorbed mercury from the biochar at different temperatures. The liberated mercury is detected by Lumex RA915. Then, the Lumex feeds the real-time mercury signal value back to the computer to generate a curve of the mercury signal changing with temperature. The mercury species adsorbed on biochar can be determined by evaluating the temperature at which the mercury species was released [29]. The following method was used for the tests: 0.1 g of adsorbed biochar

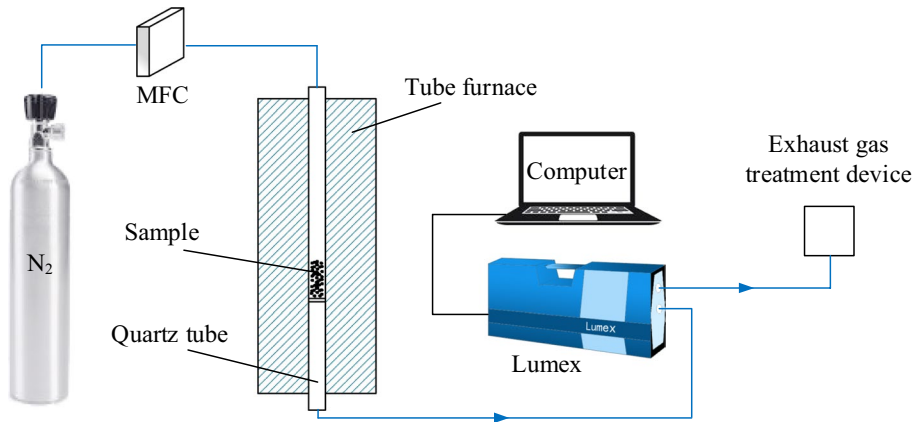


Fig. 4 Schematic diagram of the TPD device

(TS-C1, TS-C0.6, TS-C0.3, TS-BC) was placed in the TPD test bench. The temperature was increased from 20 to 500 °C at a rate of 10 °C/min, the carrier gas was nitrogen and the flow rate was 300 mL/min. The schematic diagram of the TPD device is shown in Fig. 4.

## Adsorption Kinetics

The study of mercury adsorption kinetics in flue gas is useful, and it provides a good reference for the reaction pathway and adsorption reaction mechanism. In a dynamic simulation of mercury removal, the pseudo-first-order, the pseudo-second-order, Weber–Morris and Elovich kinetic models are often used. The standard error (*SE*) of the fitting result will also be calculated.

The pseudo-first-order kinetic model equation is described as follows [30, 31]:

$$q_t = q_e(1 - e^{-k_1 t}) \quad (3)$$

The pseudo-second-order kinetic model equation is described as follows [18, 32, 33]:

$$q_t = \frac{k_2 q_e^2 t}{1 + k_2 q_e t} \quad (4)$$

where  $q_e$  represents the adsorption mass of  $\text{Hg}^0$  ( $\mu\text{g/g}$ ) at equilibrium time,  $k_1$  and  $k_2$  represent the correlation constant of the pseudo-first-order kinetic model ( $\text{min}^{-1}$ ) and the pseudo-second-order kinetic model ( $\text{g}/\mu\text{g min}$ ), respectively.

The Weber–Morris equation is calculated as follows [34]:

$$q_t = k_{id} t^{1/2} + C \quad (5)$$

where  $k_{id}$  represents the intraparticle diffusion rate constant [ $\mu\text{g}/(\text{g min}^{1/2})$ ],  $C$  is a constant that characterizes the degree of boundary layer effects ( $\mu\text{g/g}$ ).

The Elovich kinetic model is described as follows [35]:

$$q_t = \frac{1}{\beta} \ln \left( t + \frac{1}{\alpha\beta} \right) - \frac{1}{\beta} \ln \left( \frac{1}{\alpha\beta} \right) \quad (6)$$

where  $\alpha$  is the initial adsorption rate [ $\mu\text{g}/(\text{g min})$ ] and  $\beta$  is the desorption parameter ( $\mu\text{g/g}$ ).

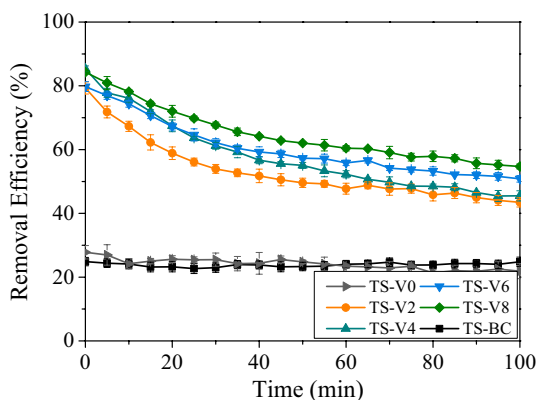
## Results and Discussion

### Adsorption Performance Under Different Discharge Voltages

The mercury adsorption performance of biochars modified under different discharge voltages is shown in Fig. 5. The mercury removal efficiency of unmodified biochar (TS-BC) is maintained at 24.8–24.6%. The initial efficiency of TS-V0 is only 3% higher than that of TS-BC. The mercury removal efficiency is significantly improved when the discharge voltage is increased to 2–8 kV. It indicates that the environment with only chlorine does not improve the mercury removal capacity of biochar. Chlorine gas still needs the assistance of plasma to modify biochar. The mercury removal efficiency of the modified bio-char gradually increases when the discharge voltage is increased from 2 to 8 kV. The biochar modified at 8 kV exhibited the best initial mercury removal efficiency at 84% and efficiency was still at 54% after 100 min. The increased voltage may be enhancing the plasma discharge effect [36], thereby increasing the amount of active chlorine gas and to form more C–Cl bond on biochar for mercury removal.

Figure 6 shows the infrared spectra of TS-BC modified using different discharge voltages. The peak at  $3400\text{ cm}^{-1}$  is attributed to an O–H stretching vibration from adsorbed water [27, 37]. The peak around  $1600\text{ cm}^{-1}$  is attributed to carboxyl stretching vibrations. The peak at  $1260\text{ cm}^{-1}$  corresponds to C–OH stretching vibrations from carboxyl groups. The data indicates that the carboxyl concentration on the biochar surface increases with increased discharge voltage. The presence of characteristic peaks at  $1090\text{ cm}^{-1}$  and  $800\text{ cm}^{-1}$  are attributed to aromatic and aliphatic C–Cl stretching vibrations, respectively [38, 39]. There was no significant change in the C–Cl intensity of TS-BC and TS-V0. As shown in Fig. 13b, the  $\text{Cl}_{2p}$  intensity of TS-V0 is not significantly enhanced and remains at the same level as TS-BC. However, the proportion of  $\text{Cl}^-$  is increased slightly, and it may be that the water in the biochar easily combines with  $\text{Cl}_2$  to form  $\text{Cl}^-$ . No significant change in the chlorine-containing functional group was responsible for the difference in mercury removal efficiency between the two samples. Compared to the non-plasma treatment sample, the peak of C–Cl increased after the chlorine plasma treatment. This indicates that chlorine combined with plasma can effectively increase the amount of C–Cl on the biochar surface. The C–Cl peak increases with the increase in discharge voltage. Considered together, the mercury removal performance data and the FTIR data for TS-V2,

**Fig. 5** Removal efficiency over time for different discharge voltages



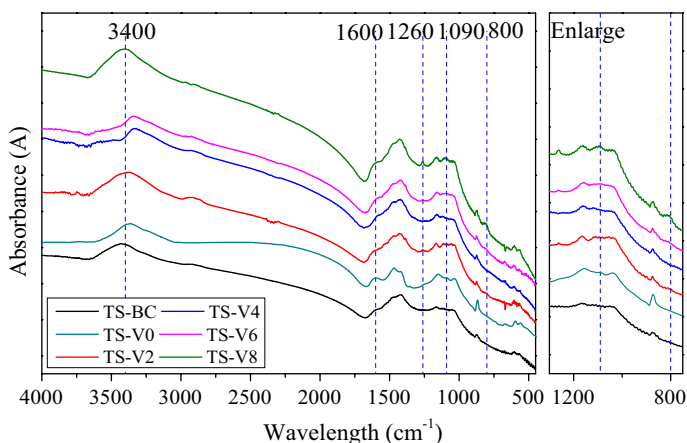


**Fig. 6** FTIR spectra of samples modified under different discharge voltages

TS-V4, TS-V6, TS-V8, indicate that increasing the discharge voltage increases the number of C–Cl bonds on the biochar surface, thereby enhancing the mercury removal effect.

Modified samples with different discharge voltages (TS-V2, TS-V4, TS-V6, TS-V8) and TS-BC were also tested by BET. The BET results are shown in Table 2. The specific surface area of TS-BC is 9.09 m<sup>2</sup>/g. Compared to commercial activated carbon, TS-BC has a very low surface area. The specific surface area of TS-BC decreased from 7.17 to 5.15 m<sup>2</sup>/g with plasma modification. This may be because the plasma has an etching effect on the biochar surface, which reduces the specific surface area.

### Adsorption Performance Under Different Discharge Times

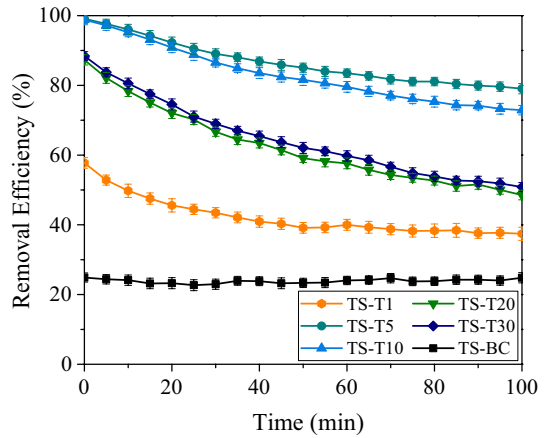
To evaluate the effect of discharge time on mercury removal efficiency, biochar was modified at 8 kV for 1 min, 5 min, 10 min, 20 min, 30 min, respectively. The results are shown in Fig. 7. When the discharge time is extended from 1 to 5 min, the initial efficiency increases from 57.7 to 99.1%. The modified biochar has the best mercury removal effect when the discharge duration is 5 min (TS-T5). Even after 100 min of mercury absorption in the fixed bed apparatus, its mercury removal efficiency is still 79%. The effect starts to drop when the discharge time exceeds 10 min. Biochar modified using a 10-min discharge time had initial mercury removal efficiency at 98.8% comparable to the 5-min discharge time biochar, but with a higher rate of decline. The initial mercury removal efficiencies for TS-T20 and TS-T30 were 87.3% and 88.4%, respectively. The decreased efficiency is

**Table 2** The specific surface area of samples

Sample	Surface area (m <sup>2</sup> /g)	R (correlation coefficient)
TS-BC	9.09	0.9999
TS-V2	7.17	0.9999
TS-V4	7.13	0.9999
TS-V6	7.06	0.9992
TS-V8	5.15	0.9997



**Fig. 7** Removal efficiency over time for different discharge times



believed to be caused by a decrease in the number of active sites on the biochar surface due to damage caused by the extended discharge time. Because plasma has high energy and high density [40]. This conclusion is supported by scanning electron microscope (SEM) data. A SEM was used to observe the surface morphology of TS-T5, TS-T10, TS-T20 and TS-T30. SEM images of these four samples are presented in Fig. 8. The surface of TS-T5 is relatively smooth with few fine particles. At the 10-min discharge time, some minor

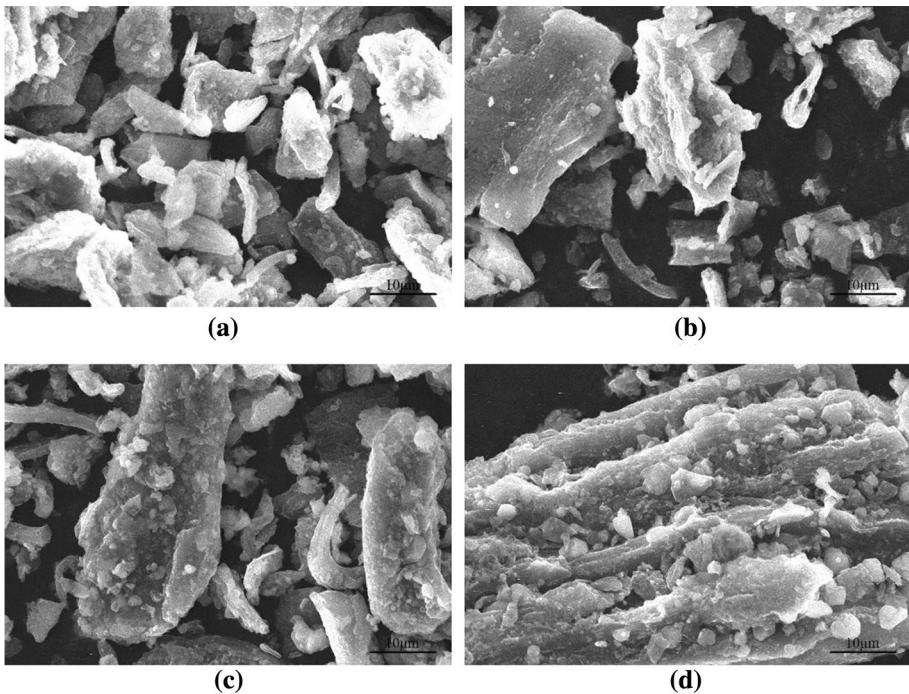


**Fig. 8** Scanning electron microscope images; **a** TS-T5; **b** TS-T10; **c** TS-T20; **d** TS-T30

grooves appeared on the biochar surface. At the 20 and 30-min discharge time, the surface started to break up. The grooves on the carbon surface became deeper and there was more granular biochar on the surface. This data supports the conclusion that long-term discharge damages the biochar surface, resulting in a decrease in mercury adsorption efficiency.

### Adsorption Performance Under Different Flow Rates

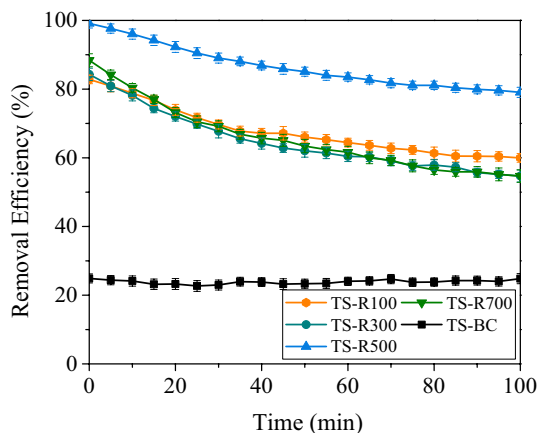
The adsorption performance under different flow rates is illustrated in Fig. 9. The initial mercury removal efficiencies were 82.8%, 84.3%, 99.1% and 88.4% at 100 mL/min, 300 mL/min, 500 mL/min and 700 mL/min, respectively. The best mercury removal efficiency was obtained using a 500 mL/min flow rate. The low mercury removal efficiencies for TS-R100 and TS-R300 could be due to the lower gas velocity didn't supply sufficient chlorine. At TS-R500, more chlorine entered the reactor and was available to react with the carbon surface. At 700 mL/min (TS-R700), the gas flow rate was so fast that the active chlorine was carried out of the reactor before it could react with the carbon surface.

Figure 10 shows the FTIR spectra for samples modified under different gas flow rates. When the gas flow rate increased from 100 and 300 to 500 mL/min, the peak intensity at  $800\text{ cm}^{-1}$  and  $1090\text{ cm}^{-1}$  increased, but decreased at 700 mL/min. This is what would be expected based upon the mercury removal efficiency data and supports the idea that the active Cl can't fully contact the biochar surface when the flow rate is too fast.

### Adsorption Performance Under Different Chlorine Concentrations

As shown in Fig. 11, mercury removal increased with increased chlorine concentration. The mercury removal efficiency of the modified sample (TS-C0) in the pure nitrogen environment was improved by 12.6% compared to TS-BC. This may be due to the fact that the  $\text{N}_2$  plasma will form an amino group on the surface of the biochar, which may be helpful for mercury removal [41]. Increasing the chlorine concentration from 0 to 1% increased the mercury removal performance from 37.4 to 99.1%. The best results were obtained using a chlorine concentration of 1%. The efficiency of TS-C1 was still at 79.1%, even after 100 min. The addition of chlorine greatly improves the modification

**Fig. 9** Removal efficiency over time for different gas flow rates



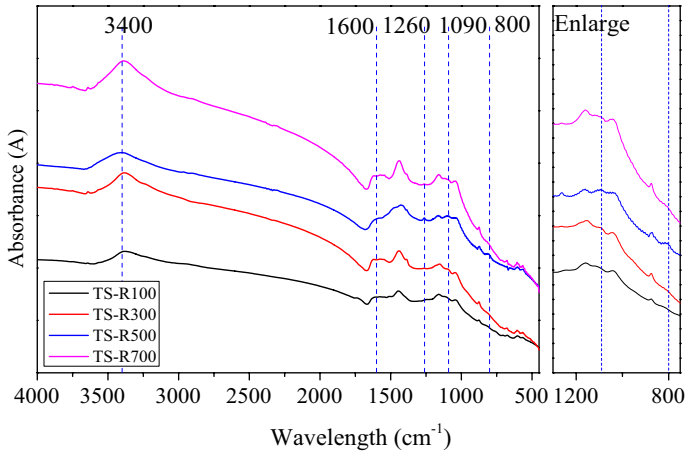
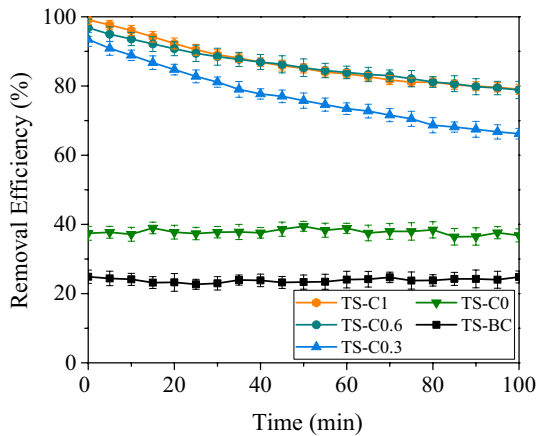


**Fig. 10** FTIR spectra of samples modified under different gas flow rates

**Fig. 11** Removal efficiency over time for different chlorine concentrations



effect with plasma assistance. There is limited room for improvement of the mercury removal effect when the concentration range is within 0.6–1%. It may be that the chlorine concentration is nearly saturated for biochar. Figure 12 shows the FTIR spectrum of the TS biochar modified under different chlorine concentrations. When the chlorine concentration is 0%, the peak area of the C–Cl bond at 1090  $\text{cm}^{-1}$  is the lowest at 0.167. As can be seen from the figure, the area of the C–Cl peak increases as the chlorine concentration enhances. The area of the C–Cl peak increased from 0.167 to 0.324 when the chlorine concentration raised from 0 to 1%. It indicates that increasing the chlorine concentration promotes the formation of C–Cl bonds on the surface of the biochar. The increase of C–Cl bond can promote the mercury removal capacity of the adsorbent.

The TC-BC, fresh TS-C1 and used TS-C1 samples were analyzed by XPS. As shown in Fig. 13a, chlorine content on the surface of fresh TS-C1 rises sharply. The chlorine atom ratio rose from 2.01 to 5.01% after modification. The peak intensity of  $\text{Cl}_{2p}$  of the modified

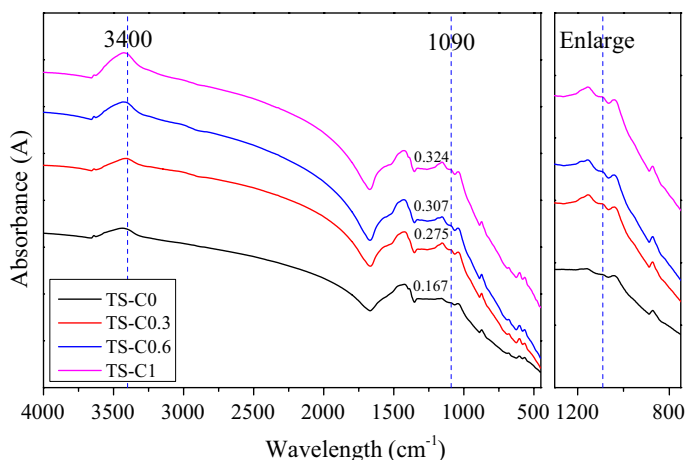


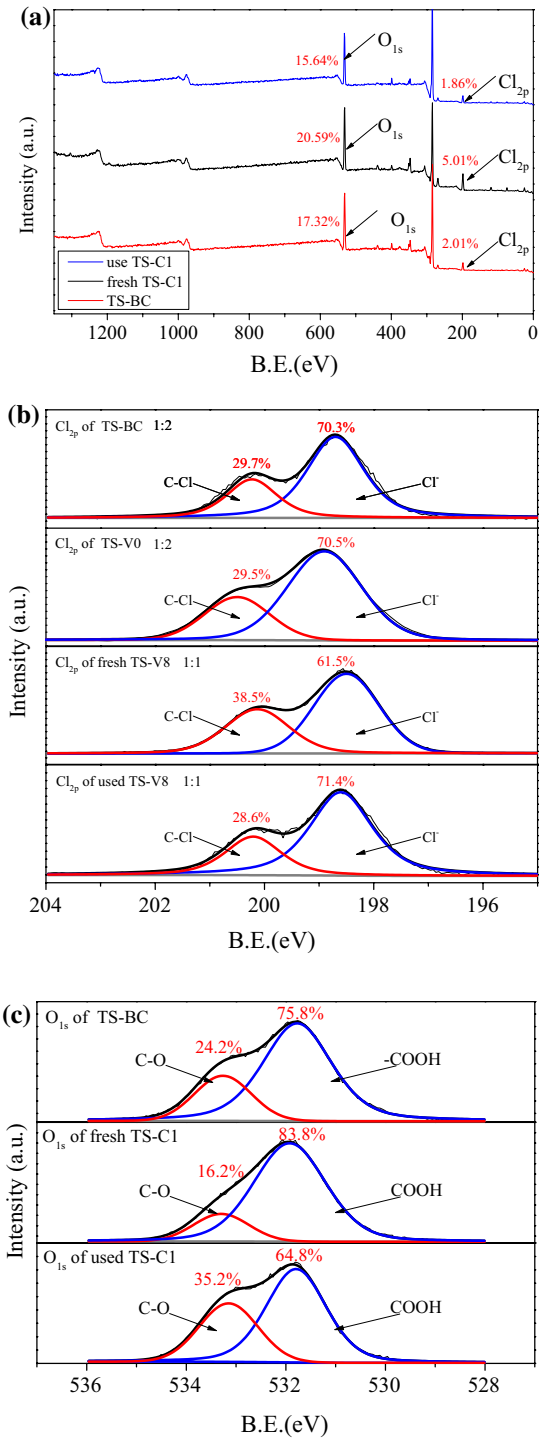
Fig. 12 FTIR spectra of samples modified under different chlorine concentration

biochar was twice that of the unmodified. The peak at this position corresponds to  $\text{Cl}^-$  and  $\text{C-Cl}$ . It suggests that the amounts of  $\text{C-Cl}$  and  $\text{Cl}^-$  was increased after chlorine plasma. The oxygen atom ratio rose from 17.32 to 20.59% after modification then decreased to 15.64% after adsorption. The raise of oxygen content after plasma modification may be due to the physical adsorption of water and oxygen by biochar. The sources of oxygen will continue to be studied in the future. The increase in chlorine atom content provides the basis for good mercury removal performance. The details of the  $\text{Cl}$  bond on the biochar surface can be obtained from the analysis of the  $\text{Cl}_{2p}$  region. Figure 13b shows a scanning diagram for the  $\text{Cl}_{2p}$  area. The  $\text{Cl}_{2p}$  spectrum of TS-BC, fresh TS-C1 and used TS-C1 is divided into two peaks. The peak at 200.2 eV is attributed to  $\text{C-Cl}$  and the peak at 198.6 eV corresponds to  $\text{Cl}^-$  [18, 25, 28]. The proportions of the two regions are shown in Table 3. After modification, the proportion of  $\text{C-Cl}$  increased from 29.7 to 38.5%. After the fresh sample is used ( $\text{Hg}^0$  adsorption for 100 min), the proportion of  $\text{C-Cl}$  dropped from 38.5 to 28.6%. This indicates that the conversion of the  $\text{C-Cl}$  bond to  $\text{Cl}^-$  supports mercury removal.

As shown in Fig. 13c, the  $\text{O}_{1s}$  curve can be separated into two peaks. One is  $\text{C-O}$  at 533.2 eV [42] and the other is  $\text{COOH}$  at 531.7 eV [43]. Table 3 provides the relative intensities of the two peaks. The proportion of  $\text{COOH}$  increased from 75.8 to 83.8% after modification but decreased to 64.8% after use. This data supports the idea that plasma promotes the formation of carboxyl groups and is in good agreement with the FTIR results. The XPS results show that carboxyl groups were consumed in mercury adsorption and played a role in the mercury removal process.

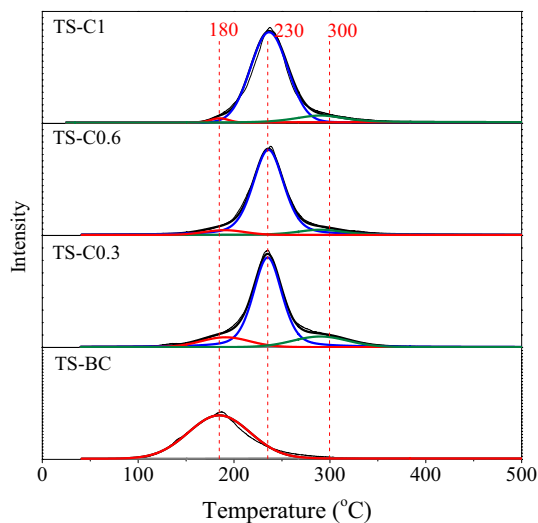
As shown in Fig. 14, the TPD curve can be divided into three peaks, 180, 230, and 300 °C respectively. The peaks at 180 °C can be attributed to  $\text{Hg}^0$  released from the biochar. The peak at around 230 °C corresponds to desorption of  $\text{HgCl}_2$  [29, 44]. The peak at around 300 °C corresponds to desorption of  $\text{HgO}$  [29, 45]. The TS-BC desorption curve indicates that the main form of  $\text{Hg}$  in TS-BC is  $\text{Hg}^0$ , which was captured by physical adsorption. In the modified biochar, the  $\text{HgCl}_2$  peak occupies a dominant position while the  $\text{Hg}^0$  peak is much lower.  $\text{Hg}^0$  may combine with  $\text{C-Cl}$  generated under chlorine plasma to form  $\text{HgCl}_2$ . From Table 4, the ratio of  $\text{Hg}^0$  decreases from 12.4 to 2.0% with the increase in chlorine concentration, while the proportion of  $\text{HgCl}_2$  increases from 68.2 to 87.5%. The

**Fig. 13** XPS spectra (a), XPS spectra of Cl<sub>2p</sub> (b) and O<sub>1s</sub> (c) for TS-BC, TS-V0, fresh TS-C1 and used TS-C1



**Table 3** Functional groups determined from XPS spectra

Functional groups	Relative intensity (%)		
	TS-BC	Fresh TS-C1	Used TS-C1
C–Cl	29.7	38.5	28.6
Cl <sup>-</sup>	70.3	61.5	71.4
C–O	24.2	16.2	35.2
COOH	75.8	83.8	64.8

**Fig. 14** Temperature programmed desorption curves**Table 4** Hg species in samples after adsorption

Species	Relative intensity (%)			
	TS-BC	TS-C0.3	TS-C0.6	TS-C1
Hg <sup>0</sup>	100	12.4	5.4	2.0
HgCl <sub>2</sub>	0	68.2	86.5	87.5
HgO	0	19.4	8.1	10.5

increased chlorine concentration increases the amount of C–Cl on the carbon surface, so that more Hg<sup>0</sup> participates in the chemical reaction to form HgCl<sub>2</sub>. The HgO peak appeared in the modified sample. This result, combined with the XPS data, indicates that Hg<sup>0</sup> was also oxidized by carboxyl groups. From the results of TPD, C–Cl is the main functional group involved in mercury removal and the carboxyl is a secondary functional group.

The in situ FTIR of Hg<sup>0</sup> adsorption by tobacco biochar after modification was also tested. The spectrum of in situ FTIR is shown in Fig. 15. The Fig. 15 exhibits the spectrum around 1090 cm<sup>-1</sup> which is attributed to C–Cl bond. The entire adsorption process lasted for 120 min. The peak area at 1090 cm<sup>-1</sup> was calculated from the software Ominic 8. The peak area at 1090 cm<sup>-1</sup> decreased from 0.0120 to 0.0103 gradually when the adsorption time was from 0 to 120 min. Therefore, the amount of C–Cl bond gradually declined as

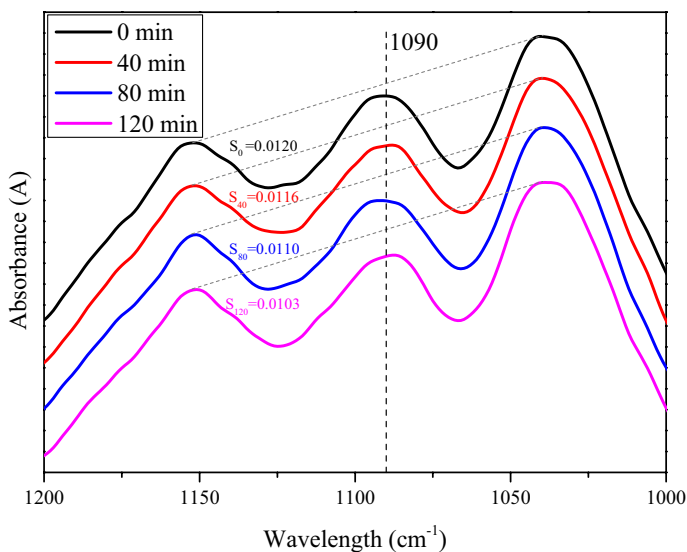


**Fig. 15** The in situ FTIR spectrum of  $\text{Hg}^0$  adsorption process

the adsorption time increases. It also suggests that the C–Cl bond generated under chlorine plasma was consumed in the Hg adsorption process.

Minitab 17 is often used to analyze the importance of product influence factors and to optimize the production process [46, 47]. The experimental parameters and efficiency were input into the Minitab software for analysis and comparison by factorial analysis. The factor analysis is a test arrangement method in which all the factors in the test are combined with each other to test the interaction effect between the main effects of each factor and factors. The influence of four factors on the mercury removal efficiency was obtained. A value greater than 2.179 indicates that a parameter can be expected to affect the experimental results significantly. As shown in Fig. 16, all influencing factors were below the significant impact boundary. The value of the standardization effect for the importance of chlorine concentration was 2.101 and is much greater than the other three parameters. This study indicates that the formation of the C–Cl bond is the most critical factor to control mercury removal efficiency. The chloride promotes the oxidation of elemental mercury into oxidized mercury and then the oxidized mercury is captured by the biochar. The flow rate, discharge time, and voltage influence the surface area or contact time with biochar. Thus, they have less effect on the removal efficiency than the chlorine concentration. The order of influence of factors on the adsorption process is: chlorine concentration > gas flow rate > discharge voltage > discharge time.

### Kinetics of Mercury Adsorption

A set of experimental results (TS-V2, TS-V4, TS-V6, TS-V8) was selected to fit with the pseudo-first-order kinetic model, the pseudo-second-order kinetic model, the Weber–Morris equation and the Elovich kinetic model. The fitting results are shown in Fig. 17 and the various fitting parameters are listed in Table 5. The error of all calculation results is

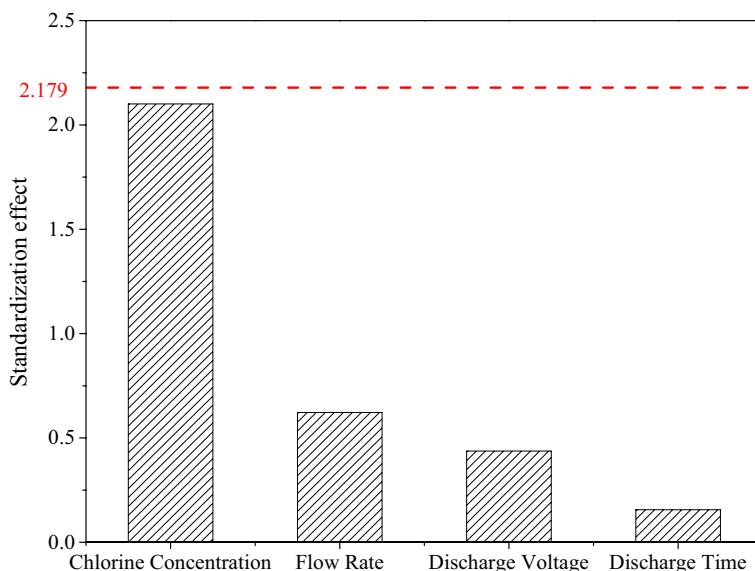


**Fig. 16** Pareto diagram of standardized effects

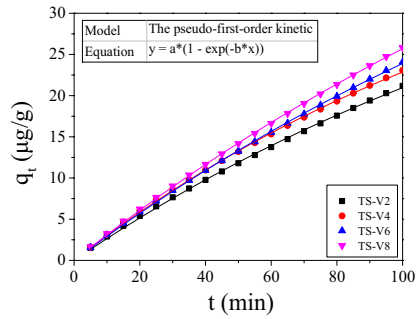
within 10%, so the result is acceptable. As observed in Fig. 17, the pseudo-first-order kinetic model and pseudo-second-order kinetic model can be fitted well with experimental data. The coefficient of determination of all fitting curves is greater than 0.999. In general, the fitting of the pseudo-second-order kinetic model is better than the pseudo-first-order kinetic model. The high degree of fitting with the pseudo-first-order kinetic equation indicates that there is an effect of external gas film diffusion during the entire adsorption process [31]. Fitted the pseudo-first-order kinetic and the pseudo-second-order kinetic model well indicates that the adsorption of mercury on the sample surface is controlled by both physical adsorption and chemical adsorption [48, 49].

The intraparticle diffusion model is poorly fitted with experimental data. The boundary layer effect constant  $C$  is not zero under all conditions, indicating that in-diffusion was not the only control step in the adsorption process. This shows that intraparticle diffusion has less effect on adsorption and the entire adsorption process is controlled by other steps. The Elovich kinetic model is generally used to describe the kinetics of chemical adsorption [35, 50, 51]. As shown in Fig. 17d, the experimental data fit well with the model indicating chemical adsorption exists in the adsorption process.

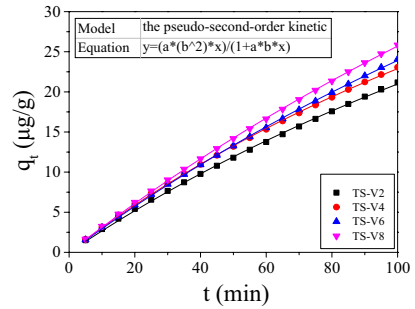
This shows that, in addition to the physical adsorption of biochar, the functional groups on the surface of biochar, especially C–Cl which obtained by modification, influence mercury removal at 30 °C. The physical adsorption and chemical adsorption processes are affected by the experimental temperature. The effect of experimental temperature changes on mercury adsorption performance will be studied later.



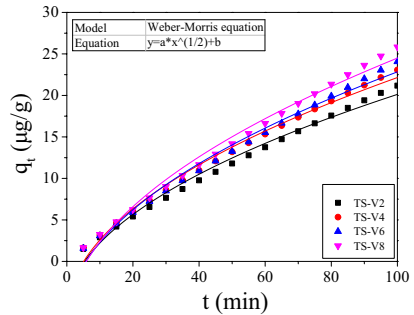
**Fig. 17** Fitting of various dynamic equations



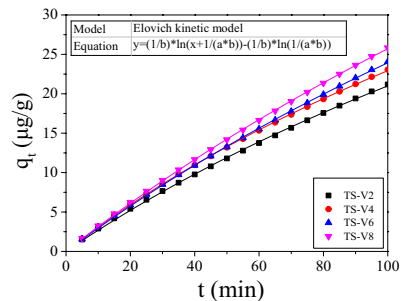
**(a)** Fitting of the pseudo-first-order kinetic



**(b)** Fitting of the pseudo-second-order kinetic



**(c)** Fitting of the Weber-Morris equation



**(d)** Fitting of the Elovich kinetic model

**Table 5** Dynamic equation fitting parameters

Sample	Pseudo-first-order model					Pseudo-second-order model				
	$q_e$	$SE$	$k_1$	$SE$	$R^2$	$q_e$	$SE$	$k_2$	$SE$	$R^2$
TS-V2	49.747	2.245	0.0055	3.04E-4	0.9993	88.193	4.053	3.540E-5	3.632E-6	0.9994
TS-V4	47.596	1.267	0.0066	2.23E-4	0.9996	82.964	2.093	4.595E-5	2.643E-6	0.9997
TS-V6	63.731	2.206	0.0047	1.95E-4	0.9997	114.960	3.937	2.285E-5	1.720E-6	0.9998
TS-V8	72.310	2.219	0.0044	1.59E-4	0.9998	131.333	3.932	1.853E-5	1.212E-6	0.9998
Sample	Weber–Morris equation					Elovich kinetic model				
	$k_{id}$	$SE$	$C$	$SE$	$R^2$	$\alpha$	$SE$	$\beta$	$SE$	$R^2$
TS-V2	2.618	0.072	-6.058	0.519	0.9859	0.279	0.003	0.026	1.214E-3	0.9995
TS-V4	2.862	0.066	-6.465	0.479	0.9899	0.321	0.002	0.028	6.530E-4	0.9998
TS-V6	3.006	0.085	-7.222	0.613	0.9851	0.305	0.002	0.019	6.588E-4	0.9998
TS-V8	3.238	0.093	-7.879	0.675	0.9845	0.322	0.001	0.016	4.921E-4	0.9999

## Conclusion

The mercury removal performance of tobacco stem biochar under different modified parameters was investigated. The results show that the influence of the four factors are ranked from large to small: chlorine concentration, gas flow rate, discharge voltage and discharge time. At a 1% chlorine concentration, the initial mercury removal efficiency was 99.1%. Both C–Cl and carboxyl increased after TS biochar modification and consumed for mercury removal. Increasing the discharge voltage increases the number of C–Cl bonds on the biochar surface, thereby enhancing the mercury removal effect. It also promotes the formation of carboxyl groups. For the discharge time, long-term discharge damages the biochar surface, resulting in a decrease in mercury adsorption efficiency. Excessive gas flow rates can result in insufficient chlorine contact time with biochar, which can reduce the amount of C–Cl. The raise in chlorine concentration increases the active site of chlorine, thereby enhancing the mercury removal effect. The results of kinetic fitting show that the mercury removal efficiency of modified TS biochar at 30 °C is controlled by physical and chemical adsorption at the same time. The mercury species present in the modified biochar after adsorption was mainly  $HgCl_2$ , with lesser amounts of  $HgO$ . The proportion of  $HgCl_2$  in the sample after adsorption is at least 68.2%. Elemental mercury was the dominate form of mercury in the unmodified biochar. Results indicate that, in addition to the C–Cl bond, the carboxyl group also participates in the mercury removal reaction. C–Cl is the most important functional group in the mercury removal process and the carboxyl is an auxiliary functional group.

**Acknowledgements** This work was supported by National Natural Science Foundation of China (51706069) and the Fundamental Research Funds for the Central Universities (2017JQ002).

## References

- Zhang Y, Mei D, Wang T, Wang J, Gu Y, Zhang Z, Romero CE, Pan W-P (2019) In-situ capture of mercury in coal-fired power plants using high surface energy fly ash. *Environ Sci Technol*. <https://doi.org/10.1021/acs.est.9b01725>

2. Rao J, Bao L, Wang B, Fan M, Feo L (2018) Plasma surface modification and bonding enhancement for bamboo composites. *Compos B Eng* 138:157–167
3. Yakut S, Ulutas K, Deger D (2018) Plasma discharge power dependent AC conductivity of plasma poly(ethylene oxide) thin films. *Thin Solid Films* 645:269–277
4. Durme JV, Dewulf J, Leys C, Langenhove HV (2008) Combining non-thermal plasma with heterogeneous catalysis in waste gas treatment: a review. *Appl Catal B* 78(3):324–333
5. Wu GQ, Zhang X, Hui H, Yan J, Zhang QS, Wan JL, Dai Y (2012) Adsorptive removal of aniline from aqueous solution by oxygen plasma irradiated bamboo based activated carbon. *Chem Eng J* 185–186(1):201–210
6. Morent R, Geyter ND, Verschuren J, Clerck KD, Kiekens P, Leys C (2008) Non-thermal plasma treatment of textiles. *Surf Coat Technol* 202(14):3427–3449
7. Lee D, Hong SH, Paek K-H, Ju W-T (2005) Adsorbability enhancement of activated carbon by dielectric barrier discharge plasma treatment. *Surf Coat Technol* 200(7):2277–2282
8. Wang T, Liu H, Zhang X, Liu J, Zhang Y, Guo Y, Sun B (2018) Catalytic conversion of NO assisted by plasma over Mn–Ce/ZSM<sub>5</sub>-multi-walled carbon nanotubes composites: investigation of acidity, activity and stability of catalyst in the synergic system. *Appl Surf Sci* 457:187–199
9. Lu L, Zheng C, Chen J, Zhou J, Xiang G, Ni M, Cen K (2015) Plasma-induced adsorption of elemental mercury on TiO<sub>2</sub> supported metal oxide catalyst at low temperatures. *Fuel Process Technol* 138:14–20
10. Yang HM, Liu H, Wu H, Wang M (2012) Photochemical removal of gaseous elemental mercury in a dielectric barrier discharge plasma reactor. *Plasma Chem Plasma Process* 32(5):969–977
11. Zhang J, Duan Y, Zhao W, Zhu C, Qiang Z, Ding W (2018) Study on elemental mercury oxidation by non-thermal plasma with calcium chloride enhancement. *Plasma Chem Plasma Process* 38(3):1–14
12. Wang ZH, Zhou JH, Zhu YQ, Wen ZC, Liu JZ, Cen K (2007) Simultaneous removal of NO<sub>x</sub>, SO<sub>2</sub> and Hg in nitrogen flow in a narrow reactor by ozone injection: experimental results. *Fuel Process Technol* 88(8):817–823
13. Zhang X, Shen B, Zhu S, Xu H, Tian L (2016) UiO-66 and its Br-modified derivatives for elemental mercury removal. *J Hazard Mater* 320:556–563
14. Stone ME, Kuehne JC, Cohen ME, Talbott JL, Scott JW (2006) Effect of iodine on mercury concentrations in dental-unit wastewater. *Dent Mater* 22(2):119–124
15. Li G, Shen B, Li Y, Zhao B, Wang F, He C, Wang Y, Zhang M (2015) Removal of element mercury by medicine residue derived biochars in presence of various gas compositions. *J Hazard Mater* 298:162–169
16. Shen B, Tian L, Li F, Zhang X, Xu H, Singh S (2017) Elemental mercury removal by the modified bio-char from waste tea. *Fuel* 187:189–196
17. Wang T, Liu J, Zhang Y, Zhang H, Chen W-Y, Norris P, Pan W-P (2018) Use of a non-thermal plasma technique to increase the number of chlorine active sites on biochar for improved mercury removal. *Chem Eng J* 331:536–544
18. Zhang B, Zeng X, Xu P, Chen J, Xu Y, Luo G, Xu M, Yao H (2016) Using the novel method of nonthermal plasma to add Cl active sites on activated carbon for removal of mercury from flue gas. *Environ Sci Technol* 50(21):11837–11843
19. Chen C, Bo L, Di L, Ogino A, Wang X, Nagatsu M (2010) Amino group introduction onto multi-walled carbon nanotubes by NH<sub>3</sub>/Ar plasma treatment. *Carbon* 48(4):939–948
20. Tsai HJ, Su YY, Tseng CC, Hsu WK (2018) Selective modification of aligned carbon nanotubes by N<sub>2</sub> plasma and their diode behavior. *RSC Adv* 8(19):10680–10685
21. Tan Z, Qiu J, Zeng H, Liu H, Xiang J (2011) Removal of elemental mercury by bamboo charcoal impregnated with H<sub>2</sub>O<sub>2</sub>. *Fuel* 90(4):1471–1475
22. Liu J, Cheney MA, Wu F, Li M (2011) Effects of chemical functional groups on elemental mercury adsorption on carbonaceous surfaces. *J Hazard Mater* 186(1):108–113
23. Zhao Y, Ma X, Xu P, Wang H, Liu Y, He A (2018) Elemental mercury removal from flue gas by CoFe<sub>2</sub>O<sub>4</sub> catalyzed peroxymonosulfate. *J Hazard Mater* 341:228–237
24. Wang F, Shen B, Gao L, Yang J (2017) Simultaneous removal of NO and Hg<sup>0</sup> from oxy-fuel combustion flue gas over CeO<sub>2</sub>-modified low-V<sub>2</sub>O<sub>5</sub>-based catalysts. *Fuel Process Technol* 168:131–139
25. Tan Z, Niu G, Chen X (2015) Removal of elemental mercury by modified bamboo carbon. *Chin J Chem Eng* 23(11):1875–1880
26. Liu Z, Yang W, Xu W, Liu Y (2018) Removal of elemental mercury by bio-chars derived from seaweed impregnated with potassium iodine. *Chem Eng J* 339:468–478
27. Johari K, Saman N, Song ST, Chin CS, Kong H, Mat H (2016) Adsorption enhancement of elemental mercury by various surface modified coconut husk as eco-friendly low-cost adsorbents. *Int Biodegrad Biodegradation* 109:45–52

28. Li G, Shen B, Li F, Tian L, Singh S, Wang F (2015) Elemental mercury removal using biochar pyrolyzed from municipal solid waste. *Fuel Process Technol* 133:43–50
29. Zhang Y, Zhao L, Guo R, Song N, Wang J, Cao Y, Orndorff W, Pan WP (2015) Mercury adsorption characteristics of HBr-modified fly ash in an entrained-flow reactor. *J Environ Sci* 33(7):156–162
30. Yang W, Liu Z, Xu W, Liu Y (2018) Removal of elemental mercury from flue gas using sargassum chars modified by  $\text{NH}_4\text{Br}$  reagent. *Fuel* 214:196–206
31. Ho YS, Mckay G (1999) Pseudo-second order model for sorption processes. *Process Biochem* 34(5):451–465
32. Ren Z, Zhu X, Du J, Kong D, Wang N, Wang Z, Wang Q, Liu W, Li Q, Zhou Z (2018) Facile and green preparation of novel adsorption materials by combining sol-gel with ion imprinting technology for selective removal of Cu(II) ions from aqueous solution. *Appl Surf Sci* 435:574–584
33. Lin J, Wang L (2009) Comparison between linear and non-linear forms of pseudo-first-order and pseudo-second-order adsorption kinetic models for the removal of methylene blue by activated carbon. *Front Environ Sci Eng China* 3(3):320–324
34. Islam M, Patel R (2011) Thermal activation of basic oxygen furnace slag and evaluation of its fluoride removal efficiency. *Chem Eng J* 169(1):68–77
35. Chien SH, Clayton WR (1980) Application of Elovich equation to the kinetics of phosphate release and sorption in soils. *Soil Sci Soc Am J* 44(2):265–268
36. Zaitsev A, Lacoste A, Poncin-Epaillard F, Bès A, Debarnot D (2017) Nanotexturing of plasma-polymer thin films using argon plasma treatment. *Surf Coat Technol* 330:196–203
37. Sun Y, Liu Y, Lou Z, Yang K, Lv D, Zhou J, Baig SA, Xu X (2018) Enhanced performance for Hg(II) removal using biomaterial (CMC/gelatin/starch) stabilized FeS nanoparticles: stabilization effects and removal mechanism. *Chem Eng J* 344:616–624
38. Hauchecorne D, Veken BJVD, Moiana A, Herrebout WA (2010) The C–Cl···N halogen bond, the weaker relative of the C–I and C–Br···N halogen bonds, finally characterized in solution. *Chem Phys* 374(1):30–36
39. Santana VT, Gonçalves SPC, Agnelli JAM, Martins-Franchetti SM (2012) Biodegradation of a polylactic acid/polyvinyl chloride blend in soil. *J Appl Polym Sci* 125(1):536–540
40. Pakpum C, Pussadee N (2016) Deep reactive ion etching of alumina titanium carbide using chlorine-based plasma. *Surf Coat Technol* 306:194–199
41. Shao D, Jiang Z, Wang X, Li J, Meng Y (2009) Plasma induced grafting carboxymethyl cellulose on multiwalled carbon nanotubes for the removal of  $\text{UO}_2(2+)$  from aqueous solution. *J Phys Chem B* 113(4):860–864
42. Pérez-Cadenas ANF, Maldonado-Hódar FJ, Moreno-Castilla C (2003) On the nature of surface acid sites of chlorinated activated carbons. *Carbon* 41(3):473–478
43. Ren X, Shao D, Zhao G, Sheng G, Hu J, Yang S, Wang X (2011) Plasma induced multiwalled carbon nanotube grafted with 2-vinylpyridine for preconcentration of Pb(II) from aqueous solutions. *Plasma Process Polym* 8(7):589–598
44. Xu Y, Zeng X, Luo G, Zhang B, Xu P, Xu M, Yao H (2016) Chlorine-char composite synthesized by co-pyrolysis of biomass wastes and polyvinyl chloride for elemental mercury removal. *Fuel* 183:73–79
45. Hassett DJ, Pflughoeft-Hassett DF, Laudal DL (1999) Mercury release from coal combustion by-products to the environment. In: *Mercury in the environment specialty conference*
46. Daiyang LI, Yang T, Yong HE, Liang L (2018) Study on the wet spinning of chitosan optimized by full factorial experiment method in Minitab software. *Adv Text Technol* 26:14–21
47. Zhuo W, Liu J, Zhang WC (2017) Research on phase change materials battery under Minitab software. *Comput Knowl Technol* 13:225–227
48. Ofomaja AE, Naidoo EB, Modise SJ (2010) Kinetic and pseudo-second-order modeling of lead biosorption onto pine cone powder. *Indengchemres* 49(6):2562–2572
49. Wu FC, Ruling T, Huang SC, Rueyshin J (2009) Characteristics of pseudo-second-order kinetic model for liquid-phase adsorption: a mini-review. *Chem Eng J* 151(1):1–9
50. Idris S, Iyaka YA, Ndamitso MM, Mohammed EB, Umar MT (2011) Evaluation of kinetic models of copper and lead uptake from dye wastewater by activated pride of barbados shell. *Am J Chem* 1(2):47–51
51. Pavlatou A, Polyzopoulos NA (2010) The role of diffusion in the kinetics of phosphate desorption: the relevance of the Elovich equation. *Eur J Soil Sci* 39(3):425–436